Temperature structure functions for air flow over moderately heated ground

K. G. Aivalis
Department of Mechanical Engineering, Yale University, New Haven, Connecticut 06520

K. R. Sreenivasan
Institute for Physical Science and Technology, University of Maryland, College Park, Maryland 20742

Y. Tsuji
Department of Energy Engineering and Science, Nagoya University, Nagoya, Aichi 4648603, Japan

J. C. Klewicki
Department of Mechanical Engineering, University of Utah, Salt Lake City, Utah 84112

C. A. Biltoft
West Desert Test Center, Dugway Proving Ground, Utah 84022

(Received 28 September 2001; accepted 19 April 2002; published 5 June 2002)

We study temperature structure functions of second, fourth, and sixth orders at heights of up to 2 m above the ground in moderately heated atmosphere. Most of the data come from measurements over salt flats of the Utah desert, with well-defined wind direction and uniform temperature boundary conditions. As in high-Rayleigh-number convection in a closed container, a thermal boundary layer develops near the ground, its thickness here being of the order of 50 cm. We demonstrate the coexistence of two scaling ranges, one of which corresponds to the classical inertial range and the other to the buoyant range influenced by thermal convection. The determination of scaling exponents in the two ranges is facilitated by the use of a scaling function. We present the variations with height of scaling exponents in both ranges, as well as the crossover scales from one range to another. © *2002 American Institute of Physics.* [DOI: 10.1063/1.1485079]

I. INTRODUCTION

Multipoint statistics in turbulent flows are of interest because they provide useful geometric information about the spatial structure (see, e.g., Ref. 1). If, for reasons of simplicity, the consideration is restricted to two-point statistics, the objects studied most are the so-called structure functions.[2] These are the moments of increments of a field variable, such as turbulent velocity and temperature, measured over a spatial separation denoted by $\mathbf{r}$. For a scalar θ, the nth order structure function is defined as

$$S_n(\mathbf{r}) = \langle (\theta(\mathbf{x}+\mathbf{r}) - \theta(\mathbf{x}))^n \rangle, \tag{1}$$

where n is an integer and $\mathbf{x}$ is the position vector. For large Reynolds numbers, it is traditionally postulated that there exists an inertial range of scales defined by $\eta \ll r \equiv |\mathbf{r}| \ll L$, where η is the Kolmogorov scale and L a large scale of the flow, in which the scaling exponents are independent of large-scale forcing and fluid viscosity. Thus, one is expected to have

$$S_n = B_n r^{\zeta_n} \tag{2}$$

where the scaling exponents ζ_n are universal and B_n may depend, at most, on the length and velocity scales of forcing (see Ref. 3 for a general discussion and Ref. 4 for the specific point on the impact of the velocity scale). In the inertial range, Antonia *et al.*,[5] Meneveau *et al.*,[6] Antonia and Smalley,[7] and Moisy *et al.*[8] are among the authors who have studied the scaling properties of temperature structure functions. These authors have measured ζ_n for conditions under which temperature can be treated essentially as a passive scalar. However, temperature is intrinsically a dynamical variable and there always exists a range of scales in which the influence of buoyancy is felt. Buoyancy manifests itself in a number of ways, e.g., in the premature truncation of the upper end of the inertial range, and in a direct influence on large scales. Studies of structure functions in the presence of substantial buoyancy have been made, among others, by Brandenburg,[9] Benzi *et al.*,[10] Cioni *et al.*,[11] Celani *et al.*,[12] and Zhou and Xia.[13] In much of this work, the difficulties associated with the small extent of the scaling range have prevented the direct determination of the scaling parameters. To overcome this problem, some of the authors cited previously have employed the extended self-similarity (ESS) technique of Benzi *et al.*[14] This technique consists of plotting structure functions of different orders against a structure function of a chosen order and obtaining a relative scaling exponent. Thus, we have

$$S_{n,\mathrm{ESS}} = S_m \zeta_m^{n,m}. \tag{3}$$

An advantage of ESS is that a reasonably convincing scaling of the form (3) can be found even when structure functions themselves obey no scaling of the form (2). We should have $\zeta_{n,m} = \zeta_n / \zeta_m$ if there is true scaling, but this cannot be asserted in general. In addition to this ambiguity of interpreta-

tion, it is not yet clear, despite several interesting efforts,[15–18] as to why ESS yields a seemingly extensive scaling even at low Reynolds numbers.

Here, we shall study the structure functions in turbulent flow over a desert that is flat for some miles, with local smoothness on scales of the order of millimeters.[19] The ground was significantly warmer than the flow above the ground, and the turbulence near the ground was driven by a combination of shear and buoyant thermal convection. The convection layer depth was estimated from measurements of optical refractive index to be of the order of 100 m. The temperature and velocity distributions near the ground have the same character as those in the temperature and velocity boundary layers in a thermal convection flow in a closed container (for two experimental studies on this extensive subject, see Refs. 20 and 21). In such studies, one defines a thermal boundary layer thickness by the distance from the walls within which most of the temperature drop occurs (see Sec. II). This layer is very thin in high-Rayleigh-number experiments (of the order of tens of microns in the extreme cases), and therefore mostly inaccessible to measurement. In the present atmospheric flow, as will be seen in Sec. II, this same measure of the thermal boundary layer thickness is of the order of 50 cm, which therefore allows some detailed measurements to be made.

The one aspect of this flow that we study here is the behavior of even-order temperature structure functions up to the sixth. The structure functions have reasonable scaling in both inertial and buoyant convective regions, which allows the determination of the scaling parameters without the use of ESS; indeed, as we shall demonstrate, the use of ESS can mask the existence of two separate scaling regions. Even where scaling is not immediately apparent, the use of a ''scaling function,'' by which is meant a functional relation that fits structure functions of any order in their entire range of scales, facilitates the determination of the scaling exponents. In this way, we shall examine the nature of scaling for heights that extend through the thermal boundary layer and somewhat beyond.

Section II is a brief summary of the measurements, while Sec. III demonstrates the existence of two ranges of scaling. The scaling function approach is discussed in Sec. IV, and the principal results are summarized in Sec. V. The concluding remarks are provided in Sec. VI.

II. MEASUREMENTS

Most measurements were made in the boundary layer above the salt flats of the Dugway Proving Ground in Utah, at different heights above the ground (1–175 cm). The ground was smooth for scales of the order of millimeters and larger, and the homogeneous terrain extended for a number of miles.[19] Temperature fluctuations were measured using a cold wire mounted on standard TSI probes. The cold wire was operated by constant current anemometer built in-house on the basis of a design by Peattie.[22] The operating current was 120 μA. The low magnitude of the current meant that the velocity contamination was minimal. The cold wires were made by etching the silver coating on a wire of platinum-10% rhodium alloy made by the Wollaston process, and the etched part had a nominal diameter of 0.6 μm and length of the order of 1 mm. After suitable amplification, the signals were low-pass filtered at 1 kHz and sampled at 2 kHz. The signals were digitized using a 12 bit analog-to-digital converter. The record lengths varied from 20 min to 1 h in real time. For these few records in which the temperature was perceptibly nonstationary, a linear detrending of the time series was performed.

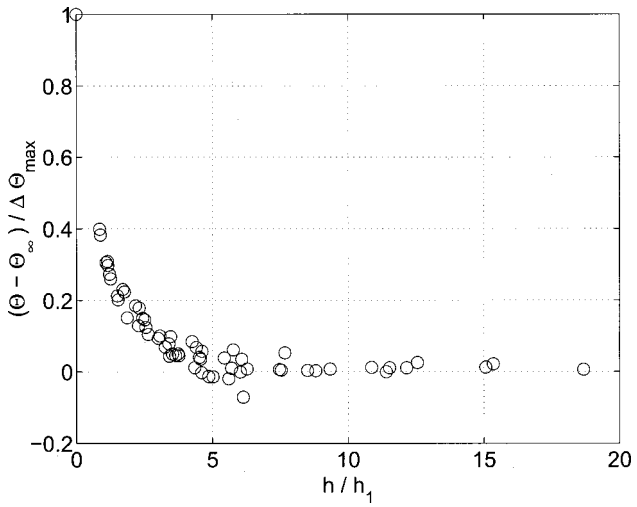

FIG. 1. The mean temperature vs h/h_1.

Some measurements were also made on the East Haven beach in Connecticut when the wind was steadily blowing from the water, but the ground conditions were not as smooth and well-controlled as in the Utah desert. The instrumentation was essentially the same. A larger share of the analysis presented here is for the desert data, but the two sets of measurements are quite consistent.

Figure 1 shows the variations of the mean temperature above the ground when the ground is warmer than the air above it. The distance from the ground is normalized by h_1, which is given by

$$h_1 = \frac{\Delta\Theta_{\max}}{\left(\frac{d\Theta}{dy}\right)^{h=0}}, \tag{4}$$

where $\Delta\Theta_{\max}$ is a nominal maximum of the (time-averaged) temperature difference between the ground and the air outside the thermal boundary layer. The height h_1 is conventionally employed in most convection studies as a measure of the thickness of the thermal boundary layer, as mentioned in Sec. I. Another useful measure of that thickness is h_2, defined somewhat arbitrarily by the position at which $\Delta\Theta$ reaches 95% of $\Delta\Theta_{\max}$. These heights as well as $\Delta\Theta_{\max}$ are listed in Table I.

We also measured the velocity fluctuations by operating an $\times$-wire on two DANTEC constant temperature anemometers. From these data, the Reynolds shear stress was computed; the friction velocity u_τ was estimated by the square-root of the maximum value of the Reynolds shear stress. The

TABLE I. Flow parameters; an ellipsis (⋯) denotes absence of reliable data. The Prandtl number is of the order of unity for all cases.

Case	h (m)	$\Delta\Theta_{max}$ (°C)	h_1 (m)	h_2 (m)	U (m/s)	u_τ (m/s)	ϵ (m^2/s^3)	η (mm)	χ ($°C^2/s$)	R_λ	$-L_{MO}$ (m)
1	0.01	1.9	0.083	0.32	5.6	0.67	0.82	0.27	0.064	2330	164.84
2	0.01	0.9	0.066	0.23	4.5	0.58	0.54	0.30	0.027	1712	528.94
3	0.035	4.0	0.10	1.00	2.2	0.27	1.0	0.26	0.76	507	25.73
4	0.095	7.0	0.10	0.81	2.0	0.27	0.23	0.37	0.87	1776	21.19
5	0.20	9.4	0.091	0.65	2.5	0.29	0.079	0.49	0.51	1997	23.80
6	0.32	9.2	0.090	0.64	2.6	0.24	0.071	0.50	0.29	3119	14.66
7	0.45	5.9	0.081	0.63	1.9	0.13	0.017	0.71	0.071	3735	4.34
8	1.40	⋯	⋯	⋯	2.25	⋯	0.0049	0.91	⋯	2900	⋯
9	1.75	⋯	⋯	⋯	0.72	⋯	⋯	⋯	⋯	⋯	⋯

mean velocity U was measured using a Pitot-tube and cross checked against the hot-wire data. These velocities are also listed in Table I.

The other basic parameters listed in Table I, as a function of the height h above the ground, are the energy dissipation rate ϵ and the scalar dissipation rate χ, both obtained by assuming local isotropy, the Kolmogorov length η, and the Monin–Obukhov length L_{MO}. Local isotropy is not accurate close to the ground but provides estimates that are better than other choices (e.g., the application of the Kolmogorov's four-fifths law[3]). The Monin–Obukhov length is an indicator of the stability of the atmosphere, and is computed here from its standard definition using the friction velocity (see Ref. 3). (In free convection studies, one often uses the Rayleigh number as an appropriate measure of buoyancy effects, but L_{MO} is a more suitable measure for present purposes. For the extreme cases of convective motion considered here, Rayleigh numbers based on the estimated convection layer height reached values as large as 10^{14}.) Although our measurements spanned both stable and unstable conditions of the atmosphere, we shall consider only the unstable conditions (i.e., $L_{MO}<0$) because we want to maintain a semblance of similarity to thermal convection. The Taylor microscale Reynolds numbers listed in Table I are thought to be sufficiently high for the inertial range properties to have attained Reynolds-number-independence.

For the analysis to follow, we use Taylor's hypothesis to convert time separation t to spatial separation r in the streamwise direction by using $Ut=r$. We avoid a discussion of its limitations here, and refer for some details to Mi and Antonia.[23]

III. THE TWO SCALING RANGES

The two scaling ranges are evident for the second-order structure function in Fig. 2, and are shown by extended dashed lines. The one toward the smaller scales is the classical inertial range, while that for larger scales is the buoyant convective range. For the same two sets of data, we show in Fig. 3 the local slopes in log–log coordinates and confirm that there indeed are two scaling ranges. The scaling exponents are the same in the two cases for the inertial range, but are different for the buoyancy range. (We will return in Sec. V to a possible explanation for this difference.) The fourth- and sixth-order structure functions, obtained from the same two sets of data, show scaling in the two regions, as displayed in Figs. 4 and 5.

We would like to demonstrate that the use of ESS in this instance—though otherwise very useful—could mask the

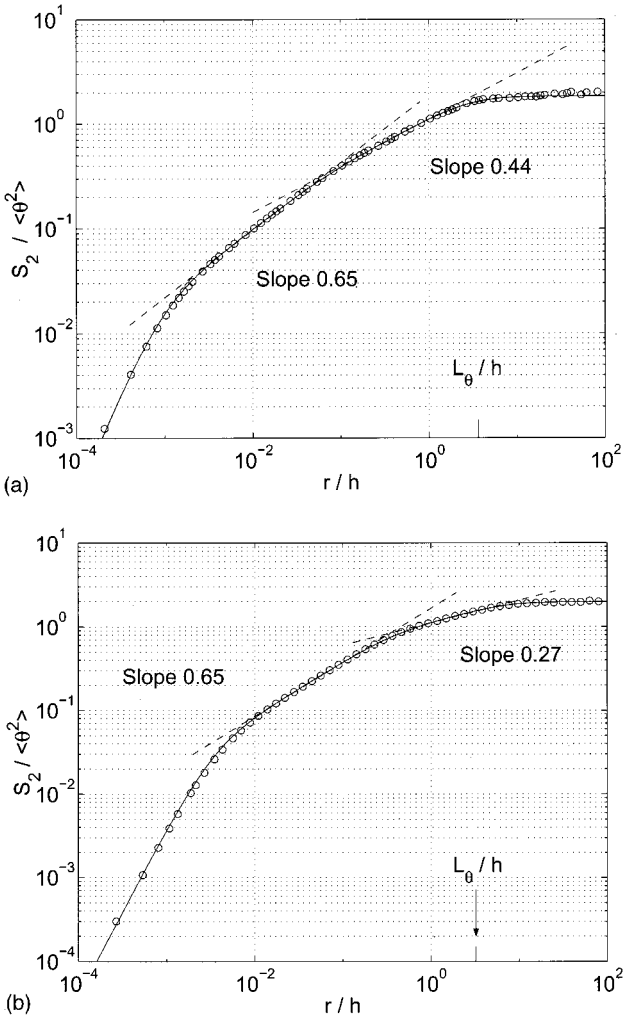

FIG. 2. The second-order structure function for temperature fluctuations for (a) or 1.75 m above the ground (Utah desert flats), and (b) 1.4 m (Connecticut beach). Shown by vertical arrows on the abscissae is the integral scale for the temperature fluctuation, L_θ, computed from the integral of the autocorrelation function and the use of Taylor's hypothesis. In all figures up to 5, as well as 7, the full line is the scaling function described in Sec. IV.

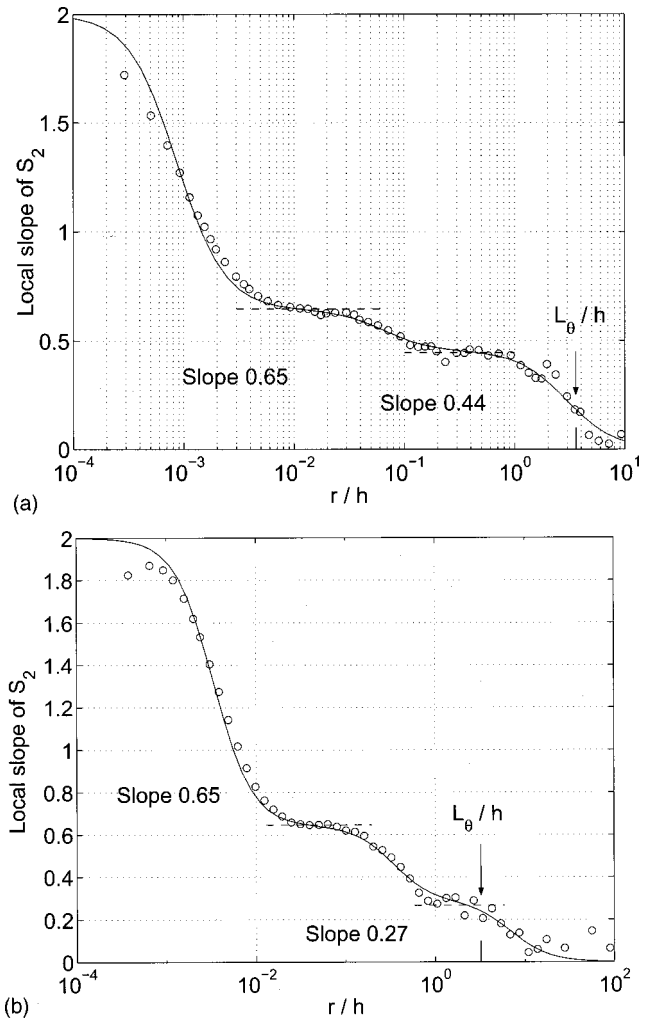

FIG. 3. The local slopes for the second-order structure function, for the same data sets used in Figs. 2(a) and 2(b). The horizontal line segments correspond to power-law fits for structure functions, and mark the extent of scaling ascribable in the log–log plots.

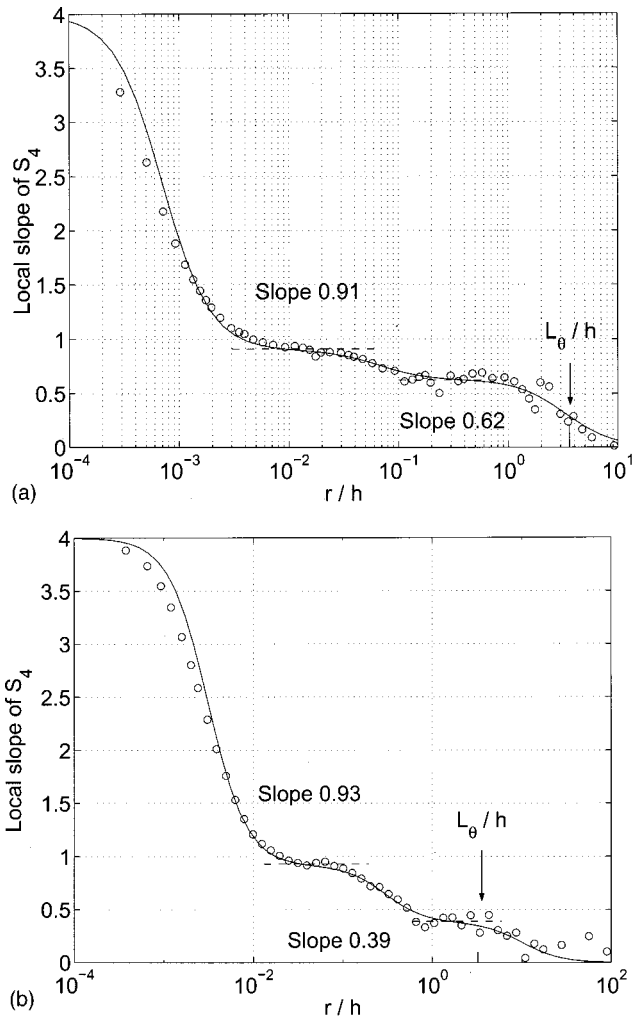

FIG. 4. The local slopes for the fourth-order structure function. The data sets are the same as in Figs. 2(a) and 2(b).

fact that there exist two scaling regions. Figure 6 shows the fourth-order structure function plotted against the second for the same two data sets as in Fig. 4. Figure 6 gives the impression of a single slope through both regions *A* and *B*, which are the two distinct scaling regions of Fig. 2. The reason for this is obviously that the ratios of the fourth-order exponent to the second-order exponent in both regions are not sufficiently different to show up as two separate lines in the ESS plot. While the data do not fall on perfect straight lines, it is clear that two distinct slopes cannot be seen in practice. (For stable conditions of the atmosphere, the two cases appear distinct even in the ESS plots, but we shall not consider them here.)

While the scaling ranges are generally clear in the two sets of data just discussed, this is not so for every case considered here. For example, for the second-order structure function shown in Fig. 7, the inertial and buoyant ranges are hardly distinguishable, and the plot of local slopes shows at best a glimmer of the two scaling regions near *A* and *B*. It is therefore useful to find an empirical expression that fits the structure functions in their entire range. From such fits, the underlying scaling can be discerned even when it may not be evident from the primitive structure functions. The point is that, even when the scaling is not obvious from the log–log plots of structure functions, these fits allow us to assign a scaling exponent and determine the cutoff scales. The underlying belief is that the scaling behavior that exists is being eroded on both sides of the scaling range—for example, by the dissipation at the low end of scaling. This approach is discussed in the following.

IV. SCALING FUNCTION APPROACH

The present approach is based on an extension of similar efforts for velocity structure functions in Refs. 7, 24, and 25. Other relevant references of the past include Refs. 26–28. One of the principal uses of the scaling function has been the extraction of the inertial range scaling exponents.

One form of the scaling function incorporating both dissipative and inertial range of scales is given by

$$S_2 = \frac{A_2 r^2}{\left(1+\left(\frac{r}{r_1}\right)^2\right)^{p_1}}. \tag{5}$$

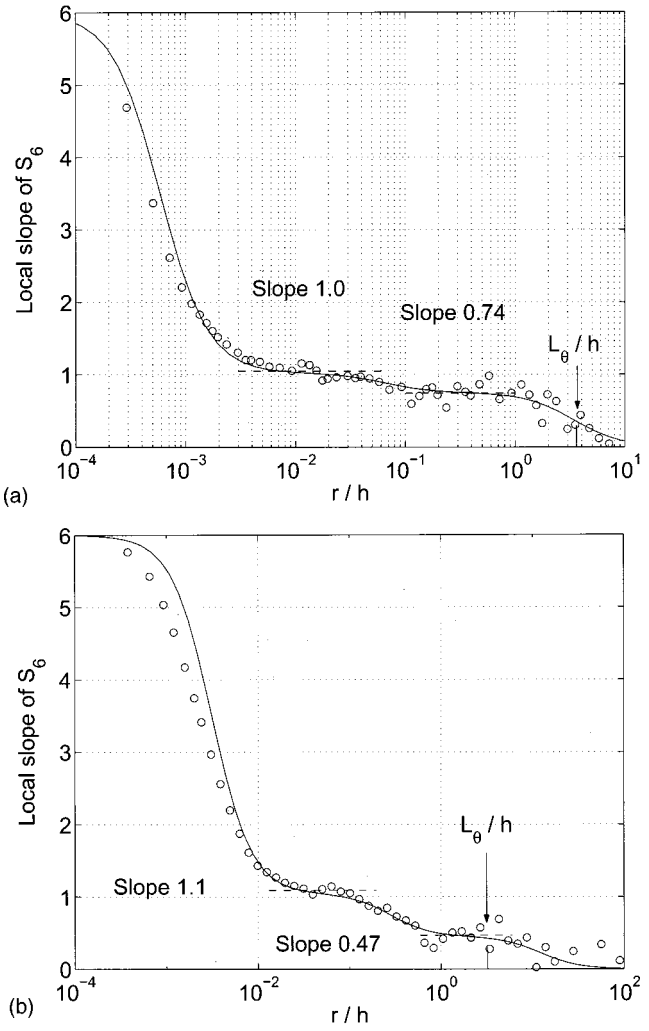

FIG. 5. The local slopes for the sixth-order structure function. The data sets are the same as in Figs. 2(a) and 2(b). While the scaling function does not fit the dissipative range of scales well in (b), it adequately fits the inertial and buoyant convective regions, these being the objects of attention here.

Here, A_2 is the mean-square temperature gradient $\langle(\partial\theta/\partial x)^2\rangle$ (see Ref. 24), r_1 is the crossover scale for the dissipative to the inertial range, and $p_1=(2-\zeta_2)/2$. To describe a second scaling range, we extend this form as

$$S_2=\frac{A_2 r^2}{\left(1+\left(\frac{r}{r_1}\right)^2\right)^{p_1}}\frac{1}{\left(1+\left(\frac{r}{r_2}\right)^2\right)^{p_2}}. \tag{6}$$

The exponent p_2 is related to the second-order scaling exponent in the buoyant convection range and r_2 represents the crossover scale between inertial and buoyancy ranges. Finally, we incorporate the property that the structure function asymptotes to a constant value for large scales, as follows:

$$S_2=\frac{A_2 r^2}{\left(1+\left(\frac{r}{r_1}\right)^2\right)^{p_1}}\frac{1}{\left(1+\left(\frac{r}{r_2}\right)^2\right)^{p_2}\left(1+\left(\frac{r}{r_3}\right)^2\right)^{p_1+p_2-1}}. \tag{7}$$

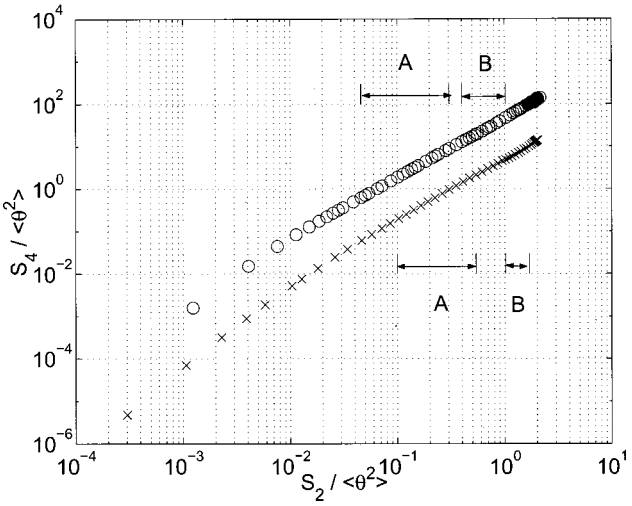

FIG. 6. The fourth-order structure function for temperature as a function of the second-order structure function. The data are the same as Figs. 2(a), circles, and 2(b), crosses. To avoid clutter, data for the former are multiplied by 10. The scaling ranges marked in Figs. 3 are shown here as intervals *A* and *B*.

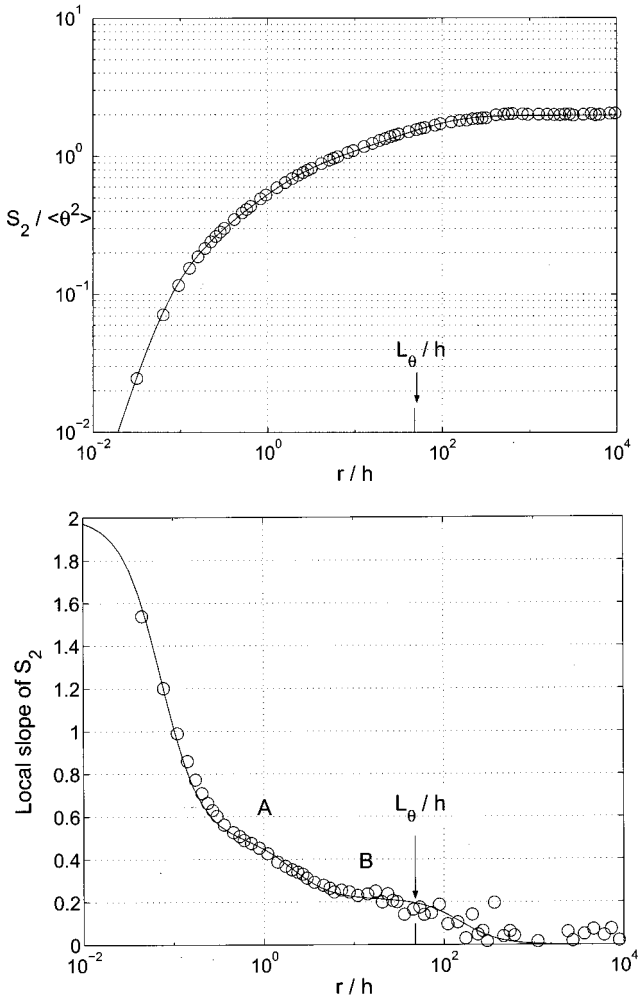

FIG. 7. The second-order structure function for temperature and its local slope as a function of the scale separation for the height of 3.5 cm from the ground.

Here r_3 is the crossover scale from the buoyancy range to where the structure functions become independent of the separation distance.

It is easy to see that Eq. (5) is equivalent for $r \gg r_1$ to

$$S_2 \sim r^{2(1-p_2)}, \tag{8}$$

while Eq. (6) is equivalent for $r \gg r_1$ and $r \ll r_2$ to

$$S_2 \sim r^{2(1-p_1)}. \tag{9}$$

Similarly, Eq. (6) is equivalent for $r \gg r_2$ and $r \ll r_3$ to

$$S_2 \sim r^{2(1-p_1-p_2)}. \tag{10}$$

In addition, for $r \gg r_3$, Eq. (7) yields

$$S_2 \sim \text{constant}, \tag{11}$$

which is consistent with the behavior in Fig. 7. In practice, this constant region shows up only when the data records are sufficiently extensive.

Formula (7) can be generalized for the nth order structure function S_n as

$$S_n = \frac{A_n r^n}{\left(1+\left(\frac{r}{r_{1n}}\right)^2\right)^{p_{1n}}} \frac{1}{\left(1+\left(\frac{r}{r_{2n}}\right)^2\right)^{p_{2n}}} \times \left(1+\left(\frac{r}{r_{3n}}\right)^2\right)^{p_{1n}+p_{2n}-n/2}. \tag{12}$$

The local slopes of the structure functions in log–log plots, based on models (5)–(7), are given, respectively, by

$$\frac{d(\log S_2)}{d(\log r)} = 2 - 2p_1 \left(\frac{r}{r_1}\right)^2 \frac{1}{1+\left(\frac{r}{r_1}\right)^2}, \tag{13}$$

$$\frac{d(\log S_2)}{d(\log r)} = 2 - 2p_1 \left(\frac{r}{r_1}\right)^2 \frac{1}{1+\left(\frac{r}{r_1}\right)^2} - 2p_2 \left(\frac{r}{r_2}\right)^2 \frac{1}{1+\left(\frac{r}{r_2}\right)^2}, \tag{14}$$

$$\frac{d(\log S_2)}{d(\log r)} = 2 - 2p_1 \left(\frac{r}{r_1}\right)^2 \frac{1}{1+\left(\frac{r}{r_1}\right)^2} - 2p_2 \left(\frac{r}{r_2}\right)^2 \frac{1}{1+\left(\frac{r}{r_2}\right)^2} + 2(p_1+p_2-1) \times \left(\frac{r}{r_3}\right)^2 \frac{1}{1+\left(\frac{r}{r_3}\right)^2}. \tag{15}$$

For the nth order structure function formula (12), the local slopes are

$$\frac{d(\log S_n)}{d(\log r)} = n - 2p_{1n} \left(\frac{r}{r_{1n}}\right)^2 \frac{1}{1+\left(\frac{r}{r_{1n}}\right)^2} - 2p_{2n} \left(\frac{r}{r_{2n}}\right)^2 \frac{1}{1+\left(\frac{r}{r_{2n}}\right)^2} + 2\left(p_{1n}+p_{2n} - \frac{n}{2}\right) \left(\frac{r}{r_{3n}}\right)^2 \frac{1}{1+\left(\frac{r}{r_{3n}}\right)^2}. \tag{16}$$

Full lines in Figs. 2–5 and 7 correspond to the fits just discussed. The curve fits follow the data more or less faithfully (with the largest discrepancies arising only in the dissipation range for the sixth order), thus enabling a reasonably trustworthy determination of the scaling exponents and cutoff scales for both scaling ranges. These results are presented and discussed in the following. They are obtained by fitting the structure functions themselves, but fitting the local slopes does not produce very different results.

V. PRINCIPAL RESULTS

Figure 8 shows the variation of the scaling exponents, for both ranges, as functions of the height from the ground. There is an increasing trend with height for $h/h_1 < 5$ (say). The exponents approach constant values far away from the ground. These basic features for all orders are the same, even though, perhaps not surprisingly, the scatter increases with the order of the exponent. (The scatter may also reflect the effects of other flow features not accounted for in this discussion.) For comparison, the Kolmogorov exponents appropriate to the inertial range are 2/3, 4/3, and 2, respectively. The measured exponents are substantially smaller, even far away from the ground. The degree of anomaly (i.e., magnitude of the departure from the Kolmogorov values) agrees with what is known from the literature, e.g., Refs. 5, 6, and 8. It is often thought (see, e.g., Ref. 11) that the buoyant convective range is governed by the considerations due to Bolgiano[29] in *stably* stratified atmosphere (see, also, Ref. 3 for a description); indeed the second-order exponent away from the ground is close to the predicted value of 0.4. But the asymptotic exponents for fourth- and sixth-order structure functions are substantially smaller than the Bolgiano values ($=0.2n$, where n is the order of the scaling exponent). There is strong anomaly also in the convective regime. At present, there is no theoretical understanding of this result.

It is now useful to return to a brief explanation of the differences in the scaling exponent in the convective regions in Figs. 2(a) and 2(b). We have shown in Fig. 8(a) that this exponent depends on the distance from the ground when the distance is small (i.e., h/h_1 less than about 5 or 10). On this basis, the data of Fig. 2(a) can be expected to correspond to h/h_1 of 5 or larger, while Fig. 2(b) to h/h_1 of about 3. The sparse mean temperature data obtained at the two sites indicate that this is likely to be the right explanation.

We now examine the variation of crossover scales as a function of h (Fig. 9). The scale r_1 varies nearly as a quarter

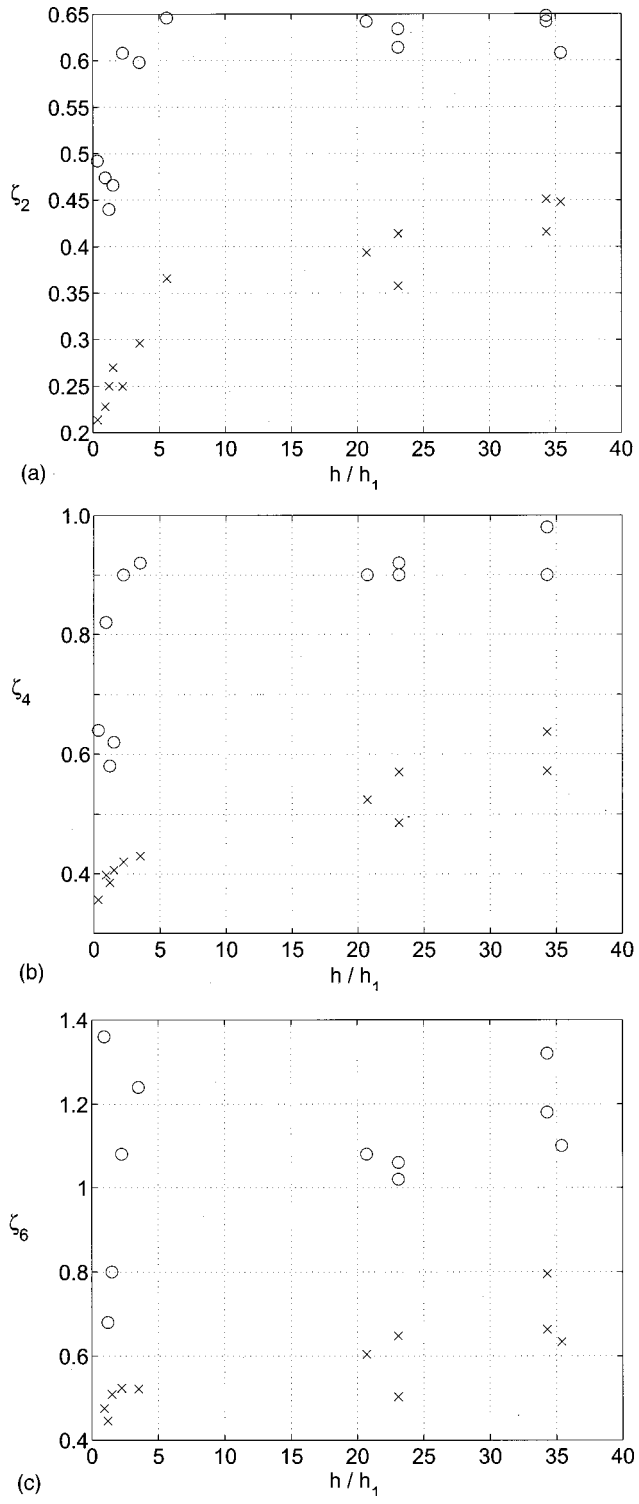

FIG. 8. The scaling exponents for the two ranges for structure functions of order 2 (a), order 4 (b), and order 6 (c). The two pairs of values for the same height correspond to two different probes at the same elevation, ×, inertial range; circles, convective range.

power of the distance above the ground, indicating that the cutoff scale between the dissipative and the inertial ranges is a multiple of the Kolmogorov scale. (This is so because a log-region present in the atmosphere implies an inverse-linear variation of the energy dissipation and a quarter-power variation of the Kolmogorov scale.[30]) The two points that lie

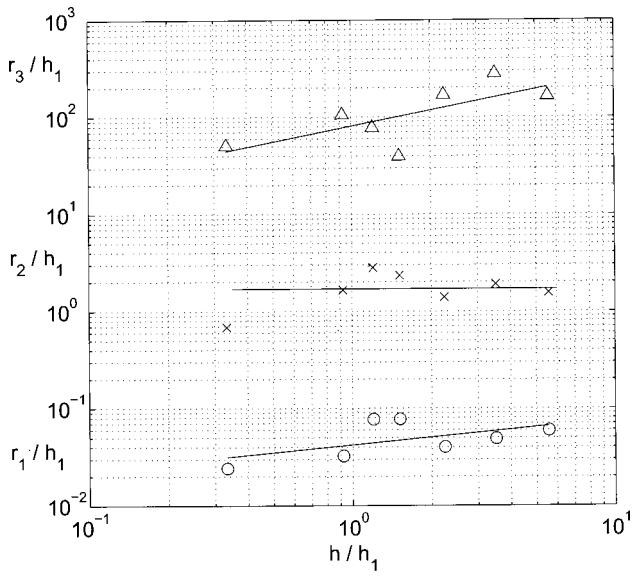

FIG. 9. The variation of the crossover scales r_1, r_2, and r_3 against the height from the ground. The slope of the fitted line for r_1 is 0.26 and for r_3 is 0.54.

above the mean line correspond to nearly neutral conditions, suggesting perhaps that the stability of the atmosphere has some bearing on the cutoff scale r_1 as well, but we do not have extensive enough data to analyze this suggestion carefully. The cutoff scale r_2, marking the boundary between the two scaling regimes, seems to scale on h_1. The present understanding (see, e.g., Ref. 11) is that this cutoff scale might correspond to the Bolgiano scale.[29] We cannot, however, confirm this assertion. The cutoff scale marking the upper end of the convective region increases with the height from the ground. We have attempted to scale r_3 by the integral scale and the Monin–Obukhov length but cannot decide on the proper scaling.

VI. CONCLUSIONS

We have explored the scaling character of temperature fluctuations within about 2 m from the ground over a hot desert. In many respects, the flow conditions here correspond to the high-Rayleigh-number convective flow in a closed container, with the difference that the thermal boundary layer can be explored in detail. We have observed two scaling ranges for the second-, fourth-, and sixth-order structure functions of temperature fluctuations. Both ranges are observed even close to the ground. High-order structure functions could not be analyzed for reasons of inadequate convergence. The classical inertial range seems to remain intact (except perhaps for a slight modification of the inner cutoff scale, r_1), and the exponents approach values appropriate to the intermittent case of isotropic turbulence. The behavior for the buoyant convective range is consistent with the observations of Zhou and Xia[13] for the thermal convection in closed containers. The exponents in this range are also strongly anomalous (i.e., significantly smaller than plausible dimensional estimates would suggest).

We have also obtained the variation of the crossover scales with the height from the ground. The scale r_1, which marks the crossover from the dissipative to inertial range, seems to scale with the Kolmogorov scale, though the numerical value may depend on the strength of convection. The scale r_2 scales with h_1, while r_3 increases with h, and appears to be influenced by buoyancy in some undetermined manner.

Finally, we wish to note that the use of ESS would diminish the distinction between the two scaling regimes, thus leading to incorrect conclusions.

ACKNOWLEDGMENTS

We are pleased to have the opportunity to show, even if on this modest scale, our appreciation to Professor John Lumley for his many contributions to our understanding of turbulence. We thank Susan Kurien and Jonathan Burt for their help with measurements and the Office of Naval Research for financial support.

[1] L. Mydlarski, A. Pumir, B. I. Shraiman, E. D. Siggia, and Z. Warhaft, "Structures and multipoint correlators for turbulent advection: Predictions and experiments," Phys. Rev. Lett. **81**, 4373 (1998).
[2] A. N. Kolmogorov, "Local structure of turbulence in an incompressible fluid for very large Reynolds numbers," Dokl. Akad. Nauk SSSR **30**, 299 (1941).
[3] A. S. Monin and A. M. Yaglom, *Statistical Fluid Mechanics* (MIT, Cambridge, 1975).
[4] K. R. Sreenivasan and B. Dhruva, "Is there scaling in high-Reynolds-number turbulence?" Prog. Theor. Phys. **130**, 103 (1998).
[5] R. A. Antonia, E. J. Hopfinger, Y. Gagne, and F. Anselmet, "Temperature structure functions in turbulent shear flows," Phys. Rev. A **30**, 2704 (1984).
[6] C. Meneveau, K. R. Sreenivasan, P. Kailasnath, and M. S. Fan, "Joint multifractal measures: Theory and applications to turbulence," Phys. Rev. A **41**, 894 (1990).
[7] R. A. Antonia and R. J. Smalley, "Velocity and temperature scaling in a rough wall boundary layer," Phys. Rev. E **62**, 640 (2000).
[8] F. Moisy, H. Willaime, J. S. Andersen, and P. Tabeling, "Passive scalar intermittency in low temperature helium flows," Phys. Rev. Lett. **86**, 4827 (2001).
[9] A. Brandenburg, "Energy spectra in a model for convective turbulence," Phys. Rev. Lett. **69**, 605 (1992).
[10] R. Benzi, R. Tripiccione, F. Massaioli, S. Succi, and S. Ciliberto, "On the scaling of the velocity and temperature structure functions in Rayleigh–Bénard convection," Europhys. Lett. **25**, 341 (1994).
[11] S. Cioni, S. Ciliberto, and J. Sommeria, "Temperature structure functions in turbulent convection at low Prandtl number," Europhys. Lett. **32**, 413 (1995).
[12] A. Celani, A. Lanotte, A. Mazzino, and M. Vergassola, "Universality and saturation of intermittency in passive scalar turbulence," Phys. Rev. Lett. **84**, 2385 (2000).
[13] S. Zhou and K. Xia, "Scaling properties of the temperature field in convective turbulence," Phys. Rev. Lett. **87**, 064501 (2001).
[14] R. Benzi, S. Ciliberto, R. Tripiccione, C. Baudet, F. Massaioli, and S. Succi, "Extended self-similarity in turbulent flows," Phys. Rev. E **48**, R29 (1993).
[15] C. Meneveau, "Transition between viscous and inertial-range scaling of turbulence structure functions," Phys. Rev. E **54**, 3687 (1996).
[16] S. Grossmann, D. Lohse, and A. Reeh, "Application of extended self-similarity in turbulence," Phys. Rev. E **56**, 5473 (1997).
[17] H. Fijisaka and S. Grossmann, "Scaling hypothesis leading to extended self-similarity in turbulence," Phys. Rev. E **63**, 026305 (2001).
[18] V. Yakhot, "Mean-field approximation and extended self-similarity in turbulence," Phys. Rev. Lett. **87**, 234501 (2001).
[19] J. C. Klewicki, J. F. Foss, and J. M. Wallace, "High Reynolds number $[R_\theta = O(10^6)]$ boundary layer turbulence in the atmospheric surface layer above western Utah's salt flats," in *Flow at Ultra-High Reynolds and Rayleigh Numbers*, edited by R. J. Donnelly and K. R. Sreenivasan (Springer, New York, 1998), pp. 450–466.
[20] J. J. Niemela, L. Skrbek, K. R. Sreenivasan, and R. J. Donnelly, "Turbulent convection in very high Rayleigh numbers," Nature (London) **404**, 837 (2000).
[21] X. Chavanne, F. Chilla, B. Chabaud, B. Castaing, and B. Hebral, "Turbulent Rayleigh–Bénard convection in gaseous and liquid He," Phys. Fluids **13**, 1300 (2001).
[22] R. Peattie, "A simple, low-drift circuit for measuring temperatures in fluids," J. Phys. E **20**, 565 (1987).
[23] J. Mi and R. A. Antonia, "Some checks of Taylor hypothesis in a slightly heated turbulent circular jet," Exp. Therm. Fluid Sci. **8**, 328 (1994).
[24] G. Stolovitzy, K. R. Sreenivasan, and A. Juneja, "Scaling functions and scaling exponents in turbulence," Phys. Rev. E **48**, R3217 (1993).
[25] B. Dhruva, Ph.D. thesis, Yale University, 2000.
[26] G. K. Batchelor, "Pressure fluctuations in isotropic turbulence," Proc. Cambridge Philos. Soc. **47**, 359 (1951).
[27] L. Sirovich, L. Smith, and V. Yakhot, "Energy spectrum of homogeneous and isotropic turbulence in far dissipation range," Phys. Rev. Lett. **72**, 344 (1994).
[28] S. Grossmann, "Asymptotic dissipation rate in turbulence," Phys. Rev. E **51**, 6275 (1995).
[29] R. Bolgiano, "Turbulent spectra in a stably stratified atmosphere," J. Geophys. Res. **64**, 2226 (1959).
[30] H. Tennekes and J. L. Lumley, *A First Course in Turbulence* (MIT, Cambridge, 1972).